Published in final edited form as:
Biochemistry. 2013 October 15; 52(41): 7350–7362. doi:10.1021/bi4009648.

Structural and chemical aspects of resistance to the antibiotic, fosfomycin, conferred by FosB from *Bacillus cereus*[†,„,‡]

Matthew K. Thompson[1], **Mary E. Keithly**[2], **Joel Harp**[3], **Paul D. Cook**[4], **Kevin L. Jagessar**[1], **Gary A. Sulikowski**[1,2], and **Richard N. Armstrong**[1,2,3,*]

[1]Department of Biochemistry, Vanderbilt University, Nashville TN 37232

[2]Department of Chemistry, Vanderbilt University, Nashville TN 37235

[3]Center for Structural Biology, Vanderbilt University, Nashville TN 37235

[4]Department of Chemistry, Grand Valley State University, Allendale MI 49401

Abstract

The fosfomycin resistance enzymes, FosB, from Gram-positive organisms, are M^{2+} dependent thiol tranferases that catalyze nucleophilic addition of either L-cysteine (L-cys) or bacillithiol (BSH) to the antibiotic, resulting in a modified compound with no bacteriacidal properties. Here we report the structural and functional characterization of FosB from *Bacillus cereus* ($FosB^{Bc}$). The overall structure of $FosB^{Bc}$, at 1.27 Å resolution, reveals that the enzyme belongs to the vicinal oxygen chelate (VOC) superfamily. Crystal structures of $FosB^{Bc}$ co-crystallized with fosfomycin and a variety of divalent metals, including Ni^{2+}, Mn^{2+}, Co^{2+}, and Zn^{2+}, indicate that the antibiotic coordinates to the active site metal center in an orientation similar to that found in the structurally homologous manganese-dependent fosfomycin resistance enzyme, FosA. Surface analysis of the $FosB^{Bc}$ structures show a well-defined binding pocket and an access channel to C1 of fosfomycin, the carbon to which nucleophilic addition of the thiol occurs. The pocket and access channel are appropriate in size and shape to accommodate L-cys or BSH. Further investigation of the structures revealed that the fosfomycin molecule, anchored by the metal, is surrounded by a cage of amino acids that hold the antibiotic in an orientation such that C1 is centered at the end of the solvent channel positioning the compound for direct nucleophilic attack by the thiol substrate. In addition, the structures of $FosB^{Bc}$ in complex with the L-cysteine-fosfomycin product (1.55 Å resolution) and in complex with the bacillithiol-fosfomycin product (1.77 Å resolution) coordinated to a Mn^{2+} metal in the active site have been determined. The L-cysteine moiety of either product is located in the solvent channel, where the thiol has added to the backside of fosfomycin C1 located at the end of the channel. Concomitant kinetic analyses of

[†]Supported by Grants R01 GM030910 to R.N.A., T32 ES007028 to M.K.T. and M.E.K., and F32 GM093507 to P.D.C. from the National Institutes of Health.

[‡]The atomic coordinates and structure factors for structures reported in this work have been deposited in the Protein Data Bank under file names 4JH1, 4JH2, 4JH3, 4JH4, 4JH5, 4JH6, 4JH7, 4JH8, and 4JH9.

[*]To whom correspondence should be addressed, Richard N. Armstrong, Department of Biochemistry, Vanderbilt University Medical Center, Nashville TN 37232, r.armstrong@vanderbilt.edu, Phone: (615) 343-2920.

Supporting Information

Additional protein figures and all x-ray fluorescence spectra are contained in the supporting information (11 figures total). This material is available free of charge via the Internet at http://pubs.acs.org.

FosB^{Bc} indicated that the enzyme has a preference for bacillithiol over L-cysteine when activated by Mn^{2+} and is inhibited by Zn^{2+}. The fact that Zn^{2+} is an inhibitor of FosB^{Bc} was used to obtain a ternary complex structure of the enzyme with both fosfomycin and L-cysteine bound.

Introduction

Microbial resistance to antibiotic compounds was recognized almost immediately after their introduction in the 1940s. The growing threat has culminated in the emergence of multiple drug resistant organisms that are invulnerable to treatment with several antimicrobial agents. While the exact mechanism of antibiotic resistance can vary, antibiotic modifying enzymes represent the most common mode of microbial survival and are, therefore, obvious targets for the development of new therapeutic agents. Combination therapies of administering antibiotics with additional enzyme inhibitors have already proven successful with the use of β-lactamase inhibitors to combat β-lactam resistant bacterial strains.

Fosfomycin, or (1*R*, 2*S*)-epoxypropylphosphonic acid, is a safe, broad-spectrum antibiotic produced by various bacteria of the genus *Streptomyces.* It was initially characterized in 1969 (1) and is used in the United States under the trade name Monurol. It is effective against both Gram-positive and Gram-negative bacteria owing to its ability to inhibit cell wall biosynthesis by inactivating the enzyme, UDP-*N*-acetylglucosamine-3-enolpyruvyltransferase or MurA. MurA catalyzes the initial step of peptidoglycan biosynthesis by transferring the enolpyruvyl moiety of phosphoenolpyruvate to the 3′-hydroxyl group of UDP-*N*-acetylglucosamine. The lactoyl moiety of the resulting UDP-*N*-acetylmuramic acid eventually provides a linker that bridges the glycan and peptide portions of peptidoglycan, an historically important target for antimicrobial agents. Fosfomycin is a phosphoenolpyruvate analog that covalently attaches to an active site cysteine of MurA, irreversibly inhibiting the enzyme and shutting down peptidoglycan biosynthesis (2–4).

Fosfomycin is most often prescribed for the treatment of urinary tract and gastrointestinal infections (5, 6). It has few human side effects and is eliminated from the body in its unmetabolized, active form. Therefore, it can be administered in a single 3 gram dose that potentially circumvents two microbial resistance mechanisms, specifically, decreased cell permeability and active efflux pumping (7). A significant disadvantage to its effectiveness, however, has been the emergence of enzymes that modify the antibiotic.

There are currently three distinct classes of fosfomycin resistance enzymes (Figure 1). **FosA** enzymes are Mn^{2+} and K^+ dependent glutathione-S-transferases that catalyze nucleophilic addition of glutathione (GSH) to C1 of fosfomycin, opening the epoxide ring of the antibiotic and resulting in a modified compound with no bactericidal properties (8–11). Genes encoding FosA have been identified in several Gram-negative bacterial species including the opportunistic human pathogen *Pseudomonas aeruginosa* (12). **FosX** enzymes are Mn^{2+} dependent hydrolases that catalyze the hydration of fosfomycin at C1 forming a vicinal diol and inactivating the antibiotic (13, 14). **FosB** enzymes were discovered in Gram-positive organisms such as *Staphylococcus aureus* and *Bacillis subtilis* (15, 16) and catalyze the M^{2+} dependent addition of L-cysteine (L-Cys) or bacillithiol to C1 of fosfomycin (17). The L-Cys transferase activity of FosB from *B. subtilis* is poor ($k_{cat}/K_M^{thiol} \sim 180\ M^{-1}s^{-1}$)

(15) when compared to the GSH transferase activity of FosA from *P. aeruginosa* ($k_{cat}/K_M^{thiol} \sim 1.7 \times 10^5\ M^{-1}s^{-1}$) (10) and is not sufficient to confer robust resistance to fosfomycin. However, recent kinetic analyses of the FosB enzymes from multiple organisms, conducted in the Armstrong laboratory, have indicated that bacillithiol is the preferred thiol substrate of the FosB enzymes *in vitro* (17).

GSH is not produced by Gram-positive bacteria, which explains why the FosB enzymes have not evolved to be glutathione-transferases. Instead, bacillithiol (BSH) is an abundant low-molecular-weight thiol found in nearly equal concentrations as L-cys. BSH (shown in Figure 2) was first isolated and identified in 2009 from *S. aureus* and *Deinococcus radiodurans* (18). Similar to the function of mycothiol in *Mycobacterium*, BSH serves as a substitute for glutathione in Gram-positive bacteria like *S. aureus* (19, 20), and BSH knockout/null cells exhibit a significant increase in their sensitivity to fosfomycin (20). FosB catalyzes addition of the cysteinyl-moiety of BSH to C1 of fosfomycin similar to FosA addition of GSH. These results have led to the FosB enzymes being classified as bacillithiol-S-transferases. The recent discovery of BSH, along with preliminary activity data, has motivated an effort to characterize the role of BSH in antimicrobial resistance of Gram-positive organisms.

Herein we report the kinetic analysis of *Bacillus cereus* ($FosB^{Bc}$) for addition of either L-cysteine or BSH to fosfomycin in the presence of Mg^{2+}, Ni^{2+}, Zn^{2+}, and Mn^{2+} and demonstrate that $FosB^{Bc}$ is a Mn^{2+} dependent thiol transferase like the homologous FosA and FosX enzymes, rather than the Mg^{2+} dependent thiol transferase originally reported (15). In addition, we demonstrate that, when activated by Mn^{2+}, $FosB^{Bc}$ has a preference for BSH over L-cys as the co-substrate for inactivation of fosfomycin, confirming that $FosB^{Bc}$ is a bacillithiol-S-transferase. Furthermore, we show that $FosB^{Bc}$ is inhibited by Zn^{2+} for either L-cys of BSH transferase activity. We also report nine three-dimensional structures of $FosB^{Bc}$. In addition to the overall structure, we have co-crystallized the enzyme with fosfomycin and several divalent metals, including Ni^{2+}, Mn^{2+}, Co^{2+}, and Zn^{2+}, tested for activation in the kinetic analyses. Moreover, we have co-crystalized the enzyme with Mn^{2+}, L-cys, and fosfomycin, as well as Mn^{2+}, BSH, and fosfomycin, to obtain either the L-cysteine-fosfomycin product [(1R,2S)-1-(S-L-cysteinyl)-2- hydroxypropylphosphonate] or the potential BS-fosfomycin [(1R,2S)-1-(S-Bacillithiolyl)-2-hydroxypropylphosphonate] product in the active site. The product structures show that the epoxide ring of fosfomycin has been opened due to nucleophilic addition of the thiol to C1 of the antibiotic. This renders the antibiotic inactive as it is no longer capable of serving as a suitable electrophilic crystalized the enzyme with Zn^{2+}, L-cys, and fosfomycin has been obtained that provides additional insight into the position of the nucleophile in the reaction.

Materials and Methods

General Materials

Buffer salts were purchased from Research Products International Corporation. All crystallization materials were from Hampton Research. Metals were obtained as their chloride salts from J.T. Baker. L-cysteine was purchased from Sigma Life Sciences. Fosfomycin disodium salt was from MP Biomedicals, LLC. BSH was synthesized as

bacillithiol disulfide (BSSB) by the Vanderbilt Chemical Synthesis Core and reduced to BSH prior to use according to published procedures (17).

Continuous ^{31}P-NMR Activity Assays with Zn^{2+} and Mg^{2+}

Intein-tagged $FosB^{Bc}$ was expressed and purified for activity assays as previously described by our lab (17). $FosB^{Bc}$ (0.5 μM) was equilibrated for 5 minutes with either 10 mM $MgCl_2$ or 100 μM $ZnCl_2$ and 8 mM fosfomycin in 20 mM HEPES (pH 7.0). The reaction was initiated by addition of 4 mM BSH or L-cys, transferred to an NMR tube, and allowed to react at room temperature. At various time points a ^{31}P with ^{1}H decoupling NMR spectra was collected using Bruker AV-400 MHz NMR. Analysis of the data was completed according to the method previously described (17).

Continuous ^{31}P-NMR Activity Assays with Ni^{2+}, Mn^{2+}, and Mg^{2}

Intein-tagged $FosB^{Bc}$ was expressed and purified for activity assays as previously described by our lab (17). $FosB^{Bc}$ (0.25 μM) was equilibrated for 5 minutes with either 1 mM $MgCl_2$, 10 μM $NiCl_2$, or 10 μM $MnCl_2$ and 4 mM fosfomycin in 20 mM HEPES (pH 7.0). The reaction was initiated by addition of 2 mM BSH or L-cys, transferred to an NMR tube, and allowed to react at room temperature. At various time points a ^{31}P with ^{1}H decoupling NMR spectra was collected using Bruker DRX-500 MHz NMR. Analysis of the data was completed according to the method previously described by our lab (17).

Protein Expression and Purification for Crystallography

A pET-20b expression plasmid containing the gene encoding non-tagged WT FosB from *Bacillus cereus* was transformed into *E. coli* BL21 (DE3) cells. See reference (17) for plasmid preparation. The cells were plated on LB-agar containing 100 ug/mL ampicillin and incubated at 37°C for approximately 16 hours. Single colonies were isolated from the LB-agar plates and used to inoculate 2 mL LB (Gibco) starter cultures (3 cultures for a total of 6 mL) containing 80 ug/mL ampicillin. After approximately 8 hours of incubation at 37°C with shaking, 1 mL of starter growth was used to inoculate 1 L of Terrific Broth containing 80 ug/ml of ampicillin (6 L total). The 1 liter cultures were grown at 37°C with shaking for approximately 12 hours (or until the OD_{600} reached ~1) and then induced with 0.5 mM IPTG. Upon induction with IPTG, the temperature was reduced to 25°C and the cells were allowed to grow for additional 4–5 hours. The cells were harvested by centrifugation at 5000 X g for 15 minutes.

The *E. coli* cell pellet was resuspended in 2 mL lysis buffer (20 mM Tris HCL, pH 7.5) per gram of cell pellet. Lysozyme was added to the slurry at 1 mg/mL, and the mixture was stirred at 4°C for 1 hour. After 1 hour of stirring, 5 mg of DNase and RNase were added and the slurry was stirred at 4°C for another hour. The slurry was sonicated to ensure complete lysing of cells and the lysate cleared by centrifugation at 35,000 X g for 30 minutes.

An ammonium sulfate precipitation was performed on the cleared lysate solution prior to any column purification. Fractions were precipitated at 5%, 20%, 40%, 60%, 80%, and 95% ammonium sulfate. The fractions were analyzed by SDS-PAGE, and fractions containing the highest ratio of FosB to other proteins were combined for further purification. The protein

was dialyzed overnight in 20 mM HEPES buffer to remove any residual lysis buffer or salt that could interfere with ion exchange chromatography.

The collected fractions were pooled, concentrated, and loaded onto a GE Healthcare HiPrep DEAE FF 16/10 column, equilibrated with 20 mM HEPES (pH 7.0) using an Amersham Pharmacia Biotech ÄKTA®*design* FPLC (equipped with a 50 mL super loop. With an estimated pI of 5.22, FosB^{Bc} adheres to the DEAE material, and a purple hue can be seen on the column. The protein was eluted from the column at 2 mL/min using a gradient of 0 – 30% NaCl in the same buffer. Fractions were analyzed for purity by SDS-PAGE. The most pure fractions were collected, combined, and dialyzed overnight into 10 mM sodium phosphate (pH 7.0).

The protein, in 10 mM sodium phosphate buffer (pH 7.0), was subsequently loaded onto a 2.5 X 15 cm hydroxyapatite column (BioRad, Hercules, CA). FosB^{Bc} adheres to the hydroxyapatite material. The protein was eluted from the column isocratically with increasing concentration of phosphate. The protein eluted between 100 and 400 mM phosphate according to fractions analyzed by SDS-PAGE.

Finally, the protein was dialyzed into 50 mM sodium phosphate buffer (pH 7.5) containing 150 mM NaCl and 5 mM DTT. The protein was concentrated to approximately 1 mL with an Amicon 10K molecular weight cutoff membrane and loaded onto a GE Healthcare 26/60 Sephacryl column at 1 mL/min using an Amersham Pharmacia Biotech FPLC. Fractions were collected from the column at 0.5 mL each and analyzed for purity by SDS-PAGE.

The purified FosB^{Bc} protein was prepared with Mn^{2+}, Ni^{2+}, and Co^{2+} by dialyzing into 50 mM Bis-Tris (pH 6.0) with 5 mM EDTA, and 2 mM 1,10-phenanthroline against 3 grams Chelex resin. This ensured removal of all metals. The protein was divided into fractions and dialyzed into 20 mM HEPES (pH 7.5) containing 200 μM of the respective divalent metal.

Protein Crystallization

Initial crystals of FosB^{Bc} were grown using the hanging drop vapor diffusion method at 298K by mixing 3 μL of protein solution (13 mg/ml in 20 mM HEPES buffer, pH 7.5) and 3 uL of reservoir solution (Hampton Research Index 92, 0.1 M magnesium formate and 15 % PEG 3350 (w/v)) in a Hampton Research VDX plate. Crystallization hits were obtained in several different conditions, but those grown in HR Index 92 yielded the best diffraction. The final optimized conditions for each crystal are as follows. For FosB^{Bc} with Zn^{2+} and sulfate and FosB^{Bc} with Zn^{2+} and fosfomycin, crystals used for SAD phasing were obtained after mixing equal volumes (3 uL) of protein solution (13 mg/ml in 20 mM HEPES buffer, pH 7.5) and the reservoir solution [0.1 M magnesium formate and 12% (w/v) polyethylene glycol 3350]. The FosB^{Bc} with Zn^{2+} and sulfate crystal used for molecular replacement was obtained after mixing equal volumes (3 uL) of protein solution (13 mg/ml in 20 mM HEPES buffer (pH 7.5), 3 mM BSH, and 5 mM DTT) and the reservoir solution [0.1 M magnesium formate and 9% (w/v) polyethylene glycol 3350]. For FosB^{Bc} with Ni^{2+}, Co^{2+}, or Mn^{2+} and fosfomycin, crystals were obtained after mixing equal volumes (3 uL) of protein solution (13 mg/ml in 20 mM HEPES buffer (pH 7.5), 5 mM fosfomycin, and 200 μM M^{2+}) and the reservoir solution [0.1 M magnesium formate and 12% (w/v) polyethylene glycol 3350, 10%

(w/v) polyethylene glycol 3350, or 12% (w/v) polyethylene glycol 3350 for Ni^{2+}, Co^{2+}, or Mn^{2+}, respectively]. For $FosB^{Bc}$ with Mn^{2+} and **2**, crystals were obtained after mixing equal volumes (3 uL) of protein solution (13 mg/ml in 20 mM HEPES buffer (pH 7.5), 5 mM fosfomycin, 5 mM L-cysteine, and 5 mM DTT; incubated for ~1 hour on ice) and the reservoir solution [0.1 M magnesium formate and 14% (w/v) polyethylene glycol 3350]. For $FosB^{Bc}$ with Zn^{2+} and L-cysteine/fosfomycin co-substrates, crystals were obtained after mixing equal volumes (3 uL) of protein solution (13 mg/ml in 20 mM HEPES buffer (pH 7.5), 5 mM fosfomycin, 5 mM L-cysteine, and 5 mM DTT; incubated for ~1 hour on ice) and the reservoir solution [0.1 M magnesium formate and 8% (w/v) polyethylene glycol 3350]. For $FosB^{Bc}$ with Mn^{2+} and **3**, crystals were obtained after mixing equal volumes (3 uL) of protein solution (13 mg/ml in 20 mM HEPES buffer (pH 7.5), 8 mM fosfomycin, 8 mM BSH, and 5 mM DTT; incubated for ~1 hour on ice) and the reservoir solution [0.1 M magnesium formate and 14% (w/v) polyethylene glycol 3350]. All crystals were cryoprotected in the mother solution and 15% glycerol prior to freezing in liquid nitrogen and data collection.

Data Collection and Refinement

Screening for the diffraction of crystals was performed at the Biomolecular Crystallography Facility in the Vanderbilt University Center for Structural Biology using a Bruker-Nonius Microstar rotating anode X-ray generator equipped with a Proteum PT135 CCD area detector mounted on an X8 kappa goniometer with Montel confocal multilayer optics. Crystals were maintained at 100K using a Bruker KryoFlex cryostat.

Diffraction data for all crystals were collected at 100 K on the LS-CAT 21-ID beamline at the APS synchrotron facility. The collected diffraction data sets were processed with HKL2000 (21). Phasing of diffraction data was done either by molecular replacement using PHASER (22) or by SAD phasing using SHELXD/E (23). For SAD phasing, presence of the anomalous scatterer was confirmed and peak wavelength determined by X-ray fluorescence. Two anomalous scatterers were located in the asymmetric unit corresponding to two active sites in the enzyme. In the case of SAD phasing, initial models were constructed using ARPwARP (24). For molecular replacement, the first model output and refined from ARPwARP was used as the initial search model. All crystals belong to the $P2_12_12_1$ space group and contain 276 amino acids in the asymmetric unit which represents the complete FosB enzyme. Manual model building for each structure was performed using *Coot* model building software (25). Waters were placed with the *Coot* routine, Find Waters. The final models were obtained by iterative cycles of model building in *Coot* and structure refinement using Refmac5 (26) in the CCP4 suite of programs (Collaborative Computational Project, 1994). All protein figures were prepared with Chimera (27). Data collection and refinement statistics are given in Table 1.

X-ray Fluorescence Spectroscopy

All x-ray fluorescence spectra of the crystals were collected at 100 K on the LS-CAT 21-ID beamline at the APS synchrotron facility and used without further processing.

Results

Kinetic Analysis

The metal activation of FosB^{Bc} by Mg^{2+} and Ni^{2+} has been reported (17). Nevertheless, divalent metal activation of the FosB enzymes remains unclear, and may be different for different organisms possessing the enzyme. In this report, kinetic analyses for the addition of either L-cysteine or BSH to fosfomycin in the presence of Mg^{2+}, Ni^{2+}, Zn^{2+}, and Mn^{2+} were conducted to further probe the appropriate divalent metal activation of FosB^{Bc} (Figure 3). Both fosfomycin and the thiol-fosfomycin product can readily be detected by ^{31}P-NMR. The initial reactions were conducted at 298 K in 20 mM HEPES (pH 7.0) with 8 mM fosfomycin and 0.5 μM FosB^{Bc} in the presence of 4 mM BSH and 10 mM Mg^{2+}, 4 mM L-cys and 10 mM Mg^{2+}, 4 mM BSH and 100 μM Zn^{2+}, or 4 mM L-Cys and 100 μM Zn^{2+} (Figure 3a). The concentration of Mg^{2+} was originally selected to be much greater than K_{act} (~200 uM) for the homologous FosB enzyme from *B.cereus* (15). The results quickly revealed that Zn^{2+} is a potent inhibitor of L-cys or BSH activity. Additional reactions to test the activity of Mn^{2+} and Ni^{2+}, along with Mg^{2+}, were conducted at 298 K in 20 mM HEPES (pH 7.0) with half the enzyme and co-substrate concentrations (Figure 3b). This was necessary because the reaction is so efficient with Mn^{2+} and BSH that the initial observable time point via the ^{31}P-NMR method using the higher concentrations was beyond completion. In addition, the concentration of Mg^{2+} was reduced to 1 mM in order to more adequately represent the prevailing intracellular concentration of the metal. Reduction of Mg^{2+} had no effect on the results. From the data, the apparent k_{cat} values for FosB^{Bc} with each metal and thiol substrate were estimated. The apparent k_{cat} values for FosB^{Bc} with BSH and Mn^{2+}, Ni^{2+}, or Mg^{2+} are 9.3 s^{-1}, 1.3 s^{-1}, and 1.0 s^{-1} respectively, and the apparent k_{cat} values for FosB^{Bc} with L-cys and Mn^{2+}, Ni^{2+}, or Mg^{2+} are 2.0 s^{-1}, 0.6 s^{-1}, and unable to be determined respectively. The results demonstrate that FosB^{Bc} has a preference for BSH over L-Cys with metal activation *in vitro* as follows: $Mn^{2+} > Ni^{2+} > Mg^{2+}$. These results indicate that FosB^{Bc} is a Mn^{2+} dependent bacillithiol-S-transferase.

Crystal Structure Determination

FosB^{Bc} with Zinc and Sulfate, SAD Phasing—(PDB 4JH1) The crystal structure of FosB^{Bc}•Zn^{2+} was refined to 1.55 Å resolution (Figure S1). The presence of a high concentration of zinc was confirmed by an x-ray fluorescence scan of the crystal prior to collection of diffraction data (Figure S2). Subsequently, the diffraction data were collected at a wavelength of 1.28 Å, the K_{α} absorption edge of Zn^{2+}, and Zn^{2+} was used to model the density.

FosB^{Bc} with Zinc and Sulfate, Molecular Replacement—(PDB 4JH2) Co-crystallization of the enzymes in the presence of BSH resulted in significantly better quality crystals even though the BSH molecule was never observed in the structure. The data set resulted in a 1.27 Å resolution structure of FosB^{Bc} with zinc and sulfate in the active site, solved by molecular replacement.

FosB^{Bc} with Zinc and Fosfomycin, SAD Phasing—(PDB 4JH3) A high resolution crystal structure of FosB^{Bc}•Zn^{2+} with fosfomycin bound to the metal ion in the active site

was obtained to 1.49 Å resolution (Figures S1 and S3). Similar to the FosB^{Bc}•Zn^{2+}•Sulfate structure (PDB 4JH1), the initial phases were determined using Zn^{2+} SAD phasing at 1.28 Å wavelength. The anomalous density map, contoured at 5σ, is displayed in Figure S3 and outlines the location of the modeled Zn^{2+} metal ions.

FosB^{Bc} with Nickel and Fosfomycin, SAD Phasing—(PDB 4JH4) A high resolution crystal structure of FosB^{Bc} with Ni^{2+} and fosfomycin bound in the active site was obtained to 1.89 Å resolution (Figure S4). The initial phases were determined using Ni^{2+} SAD phasing at 1.48 Å wavelength, the K_α absorption edge of Ni^{2+}. An x-ray fluorescence scan of the crystal prior to diffraction data collection indicated the presence of Ni^{2+} (Figure S5). The anomalous density map, modeled using Ni^{2+}, is displayed in Figure S4 and marks the location of the Ni^{2+} metal ions.

FosB^{Bc} with Cobalt and Fosfomycin, SAD Phasing—(PDB 4JH5) The crystal structure of FosB^{Bc} with Co^{2+} and fosfomycin bound in the active site was refined to 1.77 Å resolution (Figure S6). The initial phases were determined using Co^{2+} SAD phasing at 1.61 Å wavelength. Again, an x-ray fluorescence scan of the crystal prior to diffraction data collection indicated the presence of Co^{2+} (Figure S7), and the diffraction data were collected at the K_α absorption edge of Co^{2+}, 1.61 Å. Thus Co^{2+} was used to model the resulting density. The anomalous density map is displayed in Figure S6 around the modeled Co^{2+} metal ions.

FosB^{Bc} with Manganese and Fosfomycin, Molecular Replacement—(PDB 4JH6) The crystal structure of FosB^{Bc} with Mn^{2+} and fosfomycin bound in the active site was refined to 1.32 Å resolution (Figures 4 and 5a). The structure was solved by molecular replacement using the initial structure of FosB^{Bc}•Zn^{2+} where the Zn^{2+} was removed from the coordinate file before the phasing process. A SAD experimental data set was not collected for this crystal due to the 1.89 Å K_α absorption edge of Mn^{2+}. The longer wavelength can damage protein crystals during data collection. Nevertheless, an x-ray fluorescence scan of the crystal indicated the presence of Mn^{2+} (Figure S8), and because the protein was prepared with Mn^{2+} and crystallized in the same manner as that for Ni^{2+} and Co^{2+} that yielded excellent SAD phasing data, it is safe to assume that the metal ion density is that of to Mn^{2+}.

FosB^{Bc} with Manganese and L-Cysteine-Fosfomycin Product, Molecular Replacement—(PDB 4JH7) The FosB^{Bc}•Mn^{2+}•**2** product complex was obtained to 1.55 Å resolution (Figure 5b). The structure was solved by molecular replacement. The presence of Mn^{2+} in the crystal was verified by X-ray fluorescence. The B factors for each of the metal sites in the crystal indicate Mn^{2+} is a good fit for the observed electron density as the B factor for Mn^{2+} in one site is 8.1 $Å^2$ while the coordinating amino acids have average B factors of 7.9, 7.1, and 6.7 $Å^2$ for His7, His66, and Glu115, respectively. A library file in CIF format for (1R,2S)-1-(S-L-cysteinyl)-2-hydroxypropylphosphonate, was created using the online PRODRG Server (28) and inserted into the model during the final refinement.

FosB^{Bc} with Zinc, Fosfomycin, and L-cysteine, Molecular Replacement—(PDB 4JH8) The crystals of FosB^{Bc} grown in the presence of Zn^{2+}, fosfomycin, and L-cysteine

yielded electron density that is neither clearly the product nor clearly the fosfomycin and cysteine co-substrates (Figure 5c). The structure was solved by molecular replacement. The density for the C1 carbon of fosfomycin appears to be more substrate-like in character than that of the product complex (Compare Figure 5c to 5a). Moreover, there is strong electron density above C1 that is almost certainly that of sulfur. The ambiguity in the rest of the density for the cysteine likely arises from a combination of occupancy and multiple conformations in the solvent channel.

FosB^{Bc} with Mn^{2+} and Bacillithiol-Fosfomycin Product Complex, Molecular Replacement—(PDB 4JH9) The FosB^{Bc}•Mn^{2+}•**3** product complex was obtained to 1.55 Å resolution. The structure was solved by molecular replacement. The same (1R,2S)-1-(S-L-cysteinyl)-2-hydroxypropylphosphonate product was used to model the observed density in the active site because the glucosamine-malate domain of BSH was not observed (Figure S9).

Structural Characterization of FosB^{Bc}—As anticipated, the overall structure of FosB^{Bc} (Figure 4, S3, S4, and S6) reveals that the enzyme is a homodimer and belongs to the vicinal oxygen chelate (VOC) superfamily of enzymes similar to FosA, FosX (12, 13, 29), and the recently deposited FosB structure from *Bacillus anthracis* (FosB^{Ba}, PDB 4IR0). The VOC superfamily of metalloenzymes is characterized by a three-dimensional domain-swapped arrangement of tandem βαβββ-motifs, in which both subunits of the homodimer participate in coordination of each metal ion and formation of the U-shaped active sites in the enzyme (30). All of the reported structures maintain the overall arrangement with little variation. The overall RMSD for all atoms of the 9 reported FosB^{Bc} structures is 0.32 Å, calculated with Chimera (27).

Like the FosA and FosX enzymes, 2 histidines and a glutamic acid in FosB^{Bc} serve as the protein ligands that coordinate the metal ion. Specifically for FosB^{Bc}, they are His7, His66, and Glu115. In the FosB^{Bc}•Zn^{2+}•Sulfate structure (PDB 4JH2), the Zn^{2+} adopts a tetrahedral coordination geometry with a sulfate oxygen occupying the fourth-coordinate site of the inner-coordination sphere of the metal. The $2F_o$-F_c difference density calculated prior to the addition of sulfate to the coordinate file clearly establishes the presence of the sulfate ion coordinated to Zn^{2+} (Figure S1). The ligand metal distances are 2.02, 1.99, and 2.01 Å for His7, His66, and Glu115, respectively with a metal-sulfate oxygen distance of 1.90 Å.

Structure of FosB^{Bc} with M^{2+} and Fosfomycin—Coordination of fosfomycin by the various divalent metals tested is similar in each structure. The $2F_o$-F_c difference map, calculated before addition of fosfomycin to the coordinate files, clearly establishes the presence of the antibiotic coordinated to Zn^{2+} Ni^{2+}, Co^{2+}, or Mn^{2+} (PDBs 4JH1, 4JH4, 4JH5, and 4JH6; Figures 5a and S1). Similar to that observed for FosA with bound fosfomycin, the geometry of metal coordination for FosB^{Bc} with bound fosfomycin can be described as highly distorted, five-coordinate trigonal bipyramidal. His7, His66, and the phosphonate oxygen occupy the equatorial sites, while Glu115 and the oxirane oxygen of fosfomycin occupy the axial sites.

FosB^{Bc} with Mn^{2+} and L-Cysteine-Fosfomycin Product Complex and Stereochemical Configuration at C1 of the Product—The FosB^{Bc}•Mn^{2+}•**2** product complex (PDB 4JH7) was obtained in the presence of L-cys, fosfomycin, and the FosB^{Bc}•Mn^{2+} enzyme. The $2F_o$-F_c difference map outlines the product molecule in the active site of FosB^{Bc} (Figure 5b). In the structure, the epoxide ring of fosfomycin has been opened via nucleophilic addition of L-cys to C1 of fosfomycin. The C1 of fosfomycin is sp^3 hybridized and strong electron density is observed for the sulfur. The L-cys-fosfomycin product molecule was constructed in PRODRG (28) according to the stereochemistry originally reported by Bernat et al, which was biosynthesized using the FosA enzyme (31). Thus, the resulting **2** product can be correctly identified as (1R,2S)-1-(S-L-cysteinyl)-2-hydroxypropylphosphonate, the same product as that reported for FosA (31). Inversion of configuration at C1 indicates that the reaction proceeds via direct S_N2 addition of the thiol to the oxirane carbon.

The ligand metal distances in the FosB^{Bc}•Mn^{2+}•**2** structure are 2.16, 2.16, and 2.07 Å for His7, His66, and Glu115, respectively. The metal to phosphonate oxygen distance is 2.02 Å with a metal to oxirane oxygen distance of 2.36 Å.

FosB^{Bc} with Zinc and Ternary Complex, Molecular Replacement—The crystals of FosB^{Bc} grown in the presence of Zn^{2+}, fosfomycin, and L-cys yielded electron density that most closely resembles the fosfomycin and L-cys co-substrates (Figure 5c). The density for the C1 carbon of fosfomycin is more substrate-like in geometry than that of the product complex (Figure 5b). In addition, the strong electron density above C1 has a peak of 17.30 σ, too intense for even the most well-ordered water molecules. Moreover, when refined with L-cys, the sulfur atom has a B factor of 27.1 $Å^2$ averaged over the two sites. This value compares quite well with the overall B factor for the structure of 19.7 $Å^2$. Furthermore, the oxygen of Tyr39 is 3.25 Å from the sulfur, and the location of the sulfur superimposes that of the thioether of **2** in the FosB^{Bc}•Mn^{2+}•**2** structure. Finally, the distance between C1 of **1** and the sulfur is 2.79 Å. This distance is significantly shorter than the theoretical Van der Waals interaction of 3.50 Å yet much longer than a typical carbon-sulfur single bond (1.83 Å) and likely represents the location of the sulfur when it is poised for nucleophilic attack of the antibiotic. The ambiguity in the rest of the density for the L-cys probably arises from a combination of occupancy and multiple conformations throughout the crystal. Nevertheless, there is enough density to correctly establish the location of the L-cys sulfur.

This structure is not intended to serve as evidence for the location of the L-cys binding site. That location is made crystal clear by the FosB^{Bc}•Mn^{2+}•**2** structure described above. Rather, this structure is presented as a ternary structure with both substrates in the active site, an anticipated result given that Zn^{2+} is a potent inhibitor of enzymatic activity for FosB^{Bc} (Figure 3).

The most interesting aspect of this structure is the position of Asn50. The electron density for Asn50 in this structure has the residue oriented perpendicular to that of all the other structures, an orientation that positions the O_δ of Asn50 4.13 Å from C1 of fosfomycin and N_δ of Asn50 4.20 Å from the sulfur of L-cys. Superposition of the Zn^{2+}-ternary complex structure and the Mn^{2+}-product complex structure shows that, while the positions of all other

amino acids stay the same, Chi2 of Asn50 in the ternary complex is rotated approximately 90 degrees relative to the product complex (Figure 6). This structure of FosB^{Bc} is the only structure that shows significant displacement of any amino acid.

FosB^{Bc} with Mn^{2+} and BS-Fosfomycin Product Complex, Molecular Replacement—The FosB^{Bc}•Mn^{2+}•**3** product complex (PDB 4JH9) was obtained in the presence of BSH, fosfomycin, and the FosB^{Bc}•Mn^{2+} enzyme. The FosB^{Bc}•Mn^{2+}•**3** complex was determined via the same crystallization methods as those used to obtain the FosB^{Bc}•Mn^{2+}•**2** complex. FosB^{Bc} was prepared with Mn^{2+} and incubated with BSH and fosfomycin for approximately 1 hour before the solution was used for crystallization trials.

In the structure, the epoxide ring of fosfomycin has been opened via nucleophilic addition of BSH. However, electron density for the complete **3** is not observed. Rather, the electron density more closely resembles that of **2** even though L-cys was never introduced into the crystallization conditions. It is unclear if the L-cys moiety has somehow been removed from the glucosamine-malate portion of bacillithiol or if the glucosamine-malate moiety is simply not homogeneous in the crystal. Either scenario would give rise to the observed density that resembles **2** only. However, the second scenario is more plausible. First, Roberts et al. reported a purification procedure for **3** that involves heating for 10 minutes at 85°C followed by derivatization with AQC (6-aminoquinolyl-*N*-hydroxysuccinimidyl carbamate) at pH 8.8 and then adjustment to pH 5.5 for HPLC analysis (32) thereby establishing the inherent stability of **3** over a broad temperature and pH range. Second, Roberts et al. were unable to dock a BSH molecule into the crystal structure of FosB from *B. anthracis* (FosB^{Ba}, PDB 4IR0) and attributed the failure to a possible conformational change that may take place in the enzyme when BSH binds (32). Protein flexibility is critical for proper enzymatic function, and the rigidity of the crystal may prevent proper seating of the BSH molecule to the enzyme. Finally, the unit cell dimensions for this crystal (PDB 4JH9) are different than the others reported. The average unit cell dimensions for the other eight structures are 64.37 ± 0.07, 68.36 ± 0.21, and 69.96 ± 0.26 Å, while the unit cell dimensions for the crystal with **3** are 56.48, 64.48, and 83.91 Å (Table 1), indicating a significant difference in crystal packing. Given the stability of **3** and the fact that L-cys was never introduced into the crystallization conditions, it is reasonable to assume that **3** is present and simply not observed in the electron density. Thus what is observed in the structure is the phosphonate end of the product molecule tethered to the Mn^{2+} metal within the enzyme while the remainder of the molecule is solvent exposed and disordered on the surface of the enzyme within the crystal (Figure S9).

Discussion

Our initial crystals of FosB^{Bc} (PDBs 4JH1, 4JH2, and 4JH3) contained Zn^{2+} in the active site similar to the structure of FosB from *B. anthracis* (PDB 4IR0). The metal was confirmed via x-ray fluorescence and SAD phasing from the K_α edge of Zn^{2+}. These crystals were grown from preparations of FosB^{Bc} purified from cells grown in terrific broth media without further manipulation to remove or add specific metals. Therefore Zn^{2+} was the divalent metal “selected” by the enzyme from the growth conditions. Given that both our initial crystals and the crystal of FosB^{Ba} had Zn^{2+} in the active, we tested the activation of

FosB^{Bc} for both L-cys and BSH transferase activity using enzyme prepared specifically with Zn^{2+}. The results indicate that Zn^{2+} inhibits both the L-cys and BSH transferase activity of FosB^{Bc} and is ultimately what prompted further kinetic analysis of the FosB^{Bc} enzyme (Figure 3a).

Preliminary research into divalent metal activation of FosB established the activation order for FosB from *B. subtilis* as $Ni^{2+} \sim Mg^{2+} > Mn^{2+} > Fe^{2+} > Cu^{2+} > Ca^{2+} \sim Co^{2+} > Zn^{2+}$ with L-cys as the thiol substrate (15). Recent access to BSH has allowed screening of several FosB enzymes for bacillithiol-S-tranferase activity. The new results demonstrate that at least 4 known FosB enzymes, from *Staphylococcus aureus* (FosB^{Sa}), *Bacillus subtilis* (FosB^{Bs}), *Bacillus anthracis* (FosB^{Ba}), and *Bacillus cereus* (FosB^{Bc}), have a preference for BSH as the thiol substrate (17). The more extensive kinetic analysis of FosB^{Bc} presented here demonstrates a preference for BSH over L-cys and establishes the metal activation of FosB^{Bc} *in vitro* to be: $Mn^{2+} > Ni^{2+} > Mg^{2+} > Zn^{2+}$ (Figure 3a and 3b). This divalent metal activation of FosB^{Bc} is in excellent agreement with the homologous classes of fosfomycin resistance enzymes, FosA and FosX, where both are most activated by Mn^{2+} and show only very minimal activity with Zn^{2+} in the presence of their respective nucleophiles (10, 13).

The preference of FosB^{Bc} for BSH over L-cys suggests that the glucosamine-malate domain of the BSH molecule is important for substrate recognition. Substitution of the malate motif of BSH with either an *O*-methyl or *O*-benzyl aglycone group results in a 10-fold and 18-fold increase in K_M, respectively, of the substrate for FosB from *S. aureus* (32). Thus, the thermodynamic driving force of nucleophilic addition is likely interaction of the glucosamine-malate domain with the surface of the enzyme.

Surface analysis of the FosB^{Bc} structures revealed a well-defined pocket and access channel to C1 of fosfomycin, the carbon to which nucleophilic addition of the thiol occurs. The pocket and access channel are appropriate in size and shape to accommodate L-Cys or BSH. Fosfomycin is positioned in the enzyme such that the backside of the oxirane carbon to be attacked is directly centered at the end of the solvent access channel (Figure 7).

The role of the binding pocket and access channel are made clear by either the FosB^{Bc}•Mn^{2+}•**2** product complex (PDB 4JH7) or the FosB^{Bc}•Mn^{2+}•**3** product complex (PDB 4JH9). In either structure, nucleophilic addition of the thiolate to C1 of **1** has occurred at the end of the channel (Figure 8, PDB 4JH7 shown). The opening of the binding pocket from the access channel begins at the C_α end of the cysteinyl moiety where the remainder of the bacillithiol domain would be connected through the secondary amine of **3**. Unfortunately, in PDB 4JH9, the complete **3** was not observed seated in the binding pocket of the crystal for reasons described *vide supra*.

The fosfomycin molecule, coordinated to the metal, is surrounded by a cage of amino acids positioned appropriately to anchor the antibiotic in the aforementioned orientation (Figure 9). Inspection of the cage reveals it has both polar and non-polar ends to accommodate fosfomycin. The polar phosphonate group of the antibiotic is coordinated to the metal through one of the phosphonate oxygens and hydrogen bonded to Arg94, Arg124, Tyr64, and Tyr105 through the other two. The triangular cage structure around the phosphonate end

is maintained by a salt bridge from Arg94 to Asp100 and hydrogen bonds from Arg124 to Tyr39 and Asp100. On the opposite end, the oxirane oxygen is coordinated to the metal such that the methyl group of fosfomycin is held adjacent to Trp46 and C-2 of fosfomycin is "pointed" directly at Ala48. The amino acids that construct the fosmomycin cage structure and form hydrogen bonds to the antibiotic are conserved throughout all of the FosB enzymes (Figure S10, Green).

The conserved residues, Arg94 and Asp100, that form the salt bridge of the loop region in FosB that encloses the phosphonate group of fosfomycin are not found in FosA (PA1129). Rather, in FosA (PA1129) the region (approx. aa 90–100) is composed of amino acids that form the potassium binding loop. K^+ is required for optimum activation of FosA (11), but not for FosB.

Tyr39 is conserved in both the FosA and FosB enzymes. From energy-minimized docking results, Tyr39 of FosA was reported to be in a favorable position to ionize GSH, being 3.45 Å away from the docked substrate thiol (33). In both the FosB^{Bc}•Zn^{2+} ternary complex (PDB 4JH8) and the FosB^{Bc}•Mn^{2+}•**2** complex (PDB 4JH7), Tyr39 is located approximately 3.31 Å from the L-cys sulfur, consistent with the docking results for GSH to FosA. Mutation of Tyr39 to phenylalanine in FosA (PA1129) resulted in a 13-fold reduction in enzymatic turnover and a 50-fold decrease in catalytic efficiency for the thiol substrate, K_{cat}/K_M^{GSH} M (33). Thus, the function of Tyr39, in either FosA or FosB, is likely to abstract a proton from and activate the incoming thiol during the reaction. Hydrogen bonding of Tyr39 to Arg124 (see Figure 9) should stabilize the tyrosinate anion to facilitate this function.

Interestingly, the Cys9 residue of FosB^{Bc}, FosB^{Sa}, and FosB^{Ba} is not conserved in FosB^{Ss} (*Staphylococcus saprophyticus*) or FosB^{Bs} (Figure S10, Red). FosB^{Ss} has a threonine at position 9, the same as FosA (PA1129) (12). In FosA (PA1129), the Thr9 residue is proposed to activate the oxirane oxygen of fosfomycin. Similarly for FosB^{Bc}, FosB^{Sa}, and FosB^{Ba}, the Cys9 has been proposed to active the oxirane oxygen. However, in FosB^{Bs}, there is no analogous amino acid at this position that could serve to activate the fosfomycin molecule. This lack in conservation at amino acid position 9 of the FosB enzymes suggests an alternative mode of activation of the epoxide oxygen of fosfomycin rather than simply protonation by either a hydroxyl or sulfhydryl side chain as previously suggested (12).

Superposition of the FosB^{Bc}•Mn^{2+}•**1** (PDB 4JH6) and FosB^{Bc}•Mn^{2+}•**2** (PDB 4JH7) product structures provides some insight into the metal-ion assisted activation of the antibiotic. When the L-cys thiol adds to C1 of fosfomycin and the epoxide ring opens, the Mn^{2+} metal displaces from the three coordinating amino acids such that the overall coordination geometry of Mn^{2+} changes (Figures 10 and S11 and Table 2). If the Z-axis is defined along E115O_ε–Mn^{2+}– Fosfomycin-$O_{(Oxirane)}$, (Figures 11 and S11) there is a distorted trigonal bipyramidal geometry about the Mn^{2+} center similar to that observed in FosA. When the product is formed, the equatorial distances expand, and the metal-oxygen$_{(oxirane)}$ bond shortens, effectively creating a more symmetric trigonal bipyramidal geometry around Mn^{2+} and relieving strain on both the atomic orbitals of the metal and the epoxide ring of the antibiotic. The observed changes in metal-ligand bond distances are on the order of approximately 0.1 Å. These observable deviations are justified given that the estimated

overall coordinate errors from maximum likelihood refinement are 0.03 and 0.04 Å for the FosB^{Bc}•Mn^{2+}•**1** and FosB^{Bc}•Mn^{2+}•**2** structures, respectively. Furthermore, the estimated upper limits of atomic coordinate errors are 0.04 and 0.05 Å for the FosB^{Bc}•Mn^{2+}•**1** and FosB^{Bc}•Mn^{2+}•**2** structures, respectively, as calculated from Luzzati plots in the PDB validation reports.

Although the original investigation of FosB^{Bs} with L-cysteine as the thiol has a slightly different activation order, Zn^{2+} was effectively shown to be an inhibitor of L-cys transferase activity. Such similarity of metal activation by Mn^{2+} across the fosfomycin resistance enzyme classes warrants further explanation. Preferential activation of the fosfomycin resistance proteins (including FosA, FosB, and FosX) by Mn^{2+} over the other divalent transition metals tested can be explained by the hard and soft acid and base (HSAB) theory (34). In this context, Mn^{2+} is a hard acid, and the lone pair electrons on the oxirane oxygen of fosfomycin are a hard base; Ni^{2+} and Zn^{2+} are both defined as “borderline” with Zn^{2+} being the softest (34). Thus Mn^{2+} will form the strongest Lewis acid/base complex with the oxirane oxygen lone pair. Defining the Z-axis of the metal along E115O_{ε}–Mn^{2+}–Fosfomycin-$O_{(Oxirane)}$ (Figures 11 and S11) positions the d_z^2 orbital of Mn^{2+} to be the lone pair acceptor orbit. Furthermore, the lone pair on the oxirane oxygen is an excellent σ-donor for the d_z^2 orbital of Mn^{2+}, resulting in a very strong σ-type interaction between the ligand and the metal.

Strong σ donation of the epoxide lone pair into the d_z^2 orbital of Mn^{2+} will significantly increase the polarity of the C1-$O_{(Oxirane)}$ bond of fosfomycin resulting in greater partial positive charge (δ^+) on C1. In addition, the electron withdrawing nature of the phosphonate group will further enhance δ^+ on C1 through polarization of the C1-P bond. Electron charge redistribution away from C1 to both the phosphonate and the epoxide oxygen significantly increases the δ^+ on C1 and primes the antibiotic for nucleophilic attack by the thiolate substrate (Figure 11).

In the Mn^{2+}•FosB^{Bc}•**2** structure, O_{δ} of Asn50 is 3.80 Å from C1 of **2** and N_{δ} of Asn50 3.61 Å from the thioether of **2** averaged over the two active sites. These distances are on the edge of Van der Waals interactions for the nuclei. Asn50 is also conserved throughout the FosB enzymes (Figure S10, Red), but not in FosA. In FosA (PA1129), the position is occupied by a serine residue (Ser50) that has been implicated in GSH binding (33). However, in the FosB enzymes, the asparagine at position 50 likely serves to stabilize the incoming L-cys^- or BS^- negative charge, as well as the δ^+ on C1 of fosfomycin, during nucleophilic attack. Comparison of the of the Zn^{2+}•FosB^{Bc}•**1**•L-cys ternary complex and Mn^{2+}•FosB^{Bc}•**2** product structures clearly shows that Asn50 adopts two conformations, one perpendicular (ternary complex) and one nearly parallel (product complex) to the C1-S bond of the L-cys-fosfomycin product (Figure 6), the same orientation as it is observed in the other 7 structures whether fosfomycin is present or not. The latter orientation is maintained by a hydrogen bond between O_{δ} of Asn50 and the thiol of the adjacent Cys9 in the active site. Rotation of Asn50 about the C_{β}–C_{γ} bond is the only significant variation observed in the reported structures of FosB^{Bc}. The unique conformation is locked by hydrogen bonds between O_{δ} of Asn50 and the primary amine of the exogenous L-cys and between N_{δ} of Asn50 and the backbone carbonyl of Leu49. This orientation positions O_{δ} of Asn50 4.13 Å from C1 of

fosfomycin and N_δ of Asn50 4.20 Å from the L-cys thiol, well beyond Van der Waals range. Thus, in FosB^{Bc}, Tyr39 and Asn50 work in a concerted manner to ionize and stabilize the approaching thiolate during the reaction (see Figure 6).

The same rationale for why this family of fosfomycin resistance enzymes is activated by Mn^{2+} can be used to explain why the enzymes, including FosA and FosX, are least activated or even inhibited by Zn^{2+}. Zn^{2+} is the softest acid of the metals tested and will therefore form the weakest Lewis acid/base complex with the lone pair electrons of the oxirane oxygen. Furthermore, given that Zn^{2+} is a d^{10} metal species, the d_z^2 orbital is full and therefore unable to accept electron donation from the lone pair resulting in a decreased δ^+ on C1 of fosfomycin. Therefore, even though Zn^{2+} is the strongest Lewis acid of the metals tested, it will form the weakest Lewis acid/base complex with the oxirane lone pair of fosfomycin due to the energetically unfavorable soft-hard combination.

Conclusion

In summary, the mechanism of FosB^{Bc} is acid-catalyzed nucleophilic epoxide ring opening, where Mn^{2+} serves as the Lewis acid. Fosfomycin is activated by formation of a strong Lewis acid/base complex with Mn^{2+}. The resultant complex serves to enhance δ^+ on C1 through polarization of the C1-$O_{(Oxirane)}$ bond in addition to the already polarized C1-P bond of the antibiotic. Tyr39 facilitates ionization of the incoming thiol while Asn50 stabilizes both the δ^+ on C1 of fosfomycin and S^- of the incoming nucleophile. Inversion of configuration at C1 indicates that the reaction proceeds via direct S_N2 addition of the thiol to the oxirane carbon, forming the same (1R,2S)-1-(S-L-cysteinyl)-2-hydroxypropylphosphonate [or (1R,2S)-1-(S-Bacillithiolyl)-2-hydroxypropylphosphonate] product as that formed by FosA (31).

Antibiotic modifying enzymes represent a common mode of microbial resistance and are, therefore, obvious targets for the development of new therapeutic agents. Characterizing the interaction between resistance enzymes and their co-substrates is a critical step towards the discovery of lead compounds to combat antimicrobial resistant bacteria. The L-cys-fosfomycin product structure confirms the role of the solvent channel in FosB^{Bc} and represents a major contribution in understanding the mechanism of the enzyme. However, given that BSH is the preferred substrate of FosB over L-cys, part of the thermodynamic driving force of the reaction must be the interaction of the enzyme with the glucosamine-malate portion of BSH. In order to target FosB therapeutically, this interaction must still be characterized.

Supplementary Material

Refer to Web version on PubMed Central for supplementary material.

Acknowledgments

M.K.T. thanks the William N. Pearson Fellowship in Biochemistry provided by Vanderbilt University.

Use of the Advanced Photon Source, an Office of Science User Facility operated for the U.S. Department of Energy (DOE) Office of Science by Argonne National Laboratory, was supported by the U.S. DOE under Contract No.

DE-AC02-06CH11357. Use of the LS-CAT Sector 21 was supported by the Michigan Economic Development Corporation and the Michigan Technology Tri-Corridor (Grant 085P1000817).

Bibliography

1. Hendlin D, et al. Phosphonomycin, a new antibiotic produced by strains of streptomyces. Science. 1969; 166:122–123. [PubMed: 5809587]
2. Eschenburg S, Kabsch W, Healy ML, Schoenbrunn E. A New View of the Mechanisms of UDP-N-Acetylglucosamine Enolpyruvyl Transferase (MurA) and 5- Enolpyruvylshikimate-3-phosphate Synthase (AroA) Derived from X-ray Structures of Their Tetrahedral Reaction Intermediate States. J Biol Chem. 2003; 278:49215–49222. [PubMed: 13129913]
3. Eschenburg S, Priestman M, Schoenbrunn E. Evidence that the fosfomycin target Cys115 in UDP-N-acetylglucosamine enolpyruvyl transferase (MurA) is essential for product release. J Biol Chem. 2005; 280:3757–3763. [PubMed: 15531591]
4. Eschenburg S, Priestman MA, Abdul-Latif FA, Delachaume C, Fassy F, Schoenbrunn E. A Novel Inhibitor That Suspends the Induced Fit Mechanism of UDP-N- acetylglucosamine Enolpyruvyl Transferase (MurA). J Biol Chem. 2005; 280:14070–14075. [PubMed: 15701635]
5. Falagas ME, Giannopoulou KP, Kokolakis GN, Rafailidis PI. Fosfomycin: use beyond urinary tract and gastrointestinal infections. Clin Infect Dis. 2008; 46:1069–1077. [PubMed: 18444827]
6. Falagas ME, Kastoris AC, Karageorgopoulos DE, Rafailidis PI. Fosfomycin for the treatment of infections caused by multidrug-resistant non-fermenting Gram-negative bacilli: A systematic review of microbiological, animal and clinical studies. Int J Antimicrob Agents. 2009; 34:111–120. [PubMed: 19403273]
7. Patel SS, Balfour JA, Bryson HM. Fosfomycin tromethamine, A review of its antibacterial activity, pharmacokinetic properties and therapeutic efficacy as a single-dose oral treatment for acute uncomplicated lower urinary tract infections. Drugs. 1997; 53:637–656. [PubMed: 9098664]
8. Arca P, Hardisson C, Suarez JE. Purification of a glutathione S-transferase that mediates fosfomycin resistance in bacteria. Antimicrob Agents Chemother. 1990; 34:844–848. [PubMed: 2193621]
9. Arca P, Rico M, Brana AF, Villar CJ, Hardisson C, Suarez JE. Formation of an adduct between fosfomycin and glutathione: a new mechanism of antibiotic resistance in bacteria. Antimicrob Agents Chemother. 1988; 32:1552–1556. [PubMed: 3056239]
10. Bernat BA, Laughlin LT, Armstrong RN. Fosfomycin Resistance Protein (FosA) Is a Manganese Metalloglutathione Transferase Related to Glyoxalase I and the Extradiol Dioxygenases. Biochemistry. 1997; 36:3050–3055. [PubMed: 9115979]
11. Bernat BA, Laughlin LT, Armstrong RN. Elucidation of a Monovalent Cation Dependence and Characterization of the Divalent Cation Binding Site of the Fosfomycin Resistance Protein (FosA). Biochemistry. 1999; 38:7462–7469. [PubMed: 10360943]
12. Rife CL, Pharris RE, Newcomer ME, Armstrong RN. Crystal Structure of a Genomically Encoded Fosfomycin Resistance Protein (FosA) at 1.19 Å Resolution by MAD Phasing Off the L-III Edge of Tl+ J Am Chem Soc. 2002; 124:11001–11003. [PubMed: 12224946]
13. Fillgrove KL, Pakhomova S, Schaab MR, Newcomer ME, Armstrong RN. Structure and Mechanism of the Genomically Encoded Fosfomycin Resistance Protein, FosX, from Listeria monocytogenes. Biochemistry. 2007; 46:8110–8120. [PubMed: 17567049]
14. Fillgrove KL, Pakhomova S, Newcomer ME, Armstrong RN. Mechanistic Diversity of Fosfomycin Resistance in Pathogenic Microorganisms. J Am Chem Soc. 2003; 125:15730–15731. [PubMed: 14677948]
15. Cao M, Bernat BA, Wang Z, Armstrong RN, Helmann JD. FosB, a cysteine-dependent fosfomycin resistance protein under the control of σW, an extracytoplasmic-function σ factor in Bacillus subtilis. J Bacteriol. 2001; 183:2380–2383. [PubMed: 11244082]
16. Rigsby RE, Fillgrove KL, Beihoffer LA, Armstrong RN. Fosfomycin resistance proteins: a nexus of glutathione transferases and epoxide hydrolases in a metalloenzyme superfamily. Methods Enzymol. 2005; 401:367–379. [PubMed: 16399398]

17. Lamers AP, Keithly ME, Kim K, Cook PD, Stec DF, Hines KM, Sulikowski GA, Armstrong RN. Synthesis of bacillithiol and the catalytic selectivity of FosB-type fosfomycin resistance proteins. Org Lett. 2012; 14:5207–5209. [PubMed: 23030527]

18. Newton GL, Rawat M, La CJJ, Jothivasan VK, Budiarto T, Hamilton CJ, Claiborne A, Helmann JD, Fahey RC. Bacillithiol is an antioxidant thiol produced in bacilli. Nat Chem Biol. 2009; 5:625–627. [PubMed: 19578333]

19. Newton GL, Fahey RC, Rawat M. Detoxification of toxins by bacillithiol in Staphylococcus aureus. Microbiology. 2012; 158:1117–1126. [PubMed: 22262099]

20. Gaballa A, Newton GL, Antelmann H, Parsonage D, Upton H, Rawat M, Claiborne A, Fahey RC, Helmann JD. Biosynthesis and functions of bacillithiol, a major low-molecular-weight thiol in bacilli. Proc Natl Acad Sci U S A. 2010; 107:6482–6486. S6482/6481–S6482/6419. [PubMed: 20308541]

21. Otwinowski Z, Minor W. Processing of x-ray diffraction data collected in oscillation mode. Methods Enzymol. 1997; 276:307–326.

22. McCoy AJ, Grosse-Kunstleve RW, Adams PD, Winn MD, Storoni LC, Read RJ. Phaser crystallographic software. J Appl Crystallogr. 2007; 40:658–674. [PubMed: 19461840]

23. Sheldrick GM. A short history of SHELX. Acta Crystallogr A. 2008; 64:112–122. [PubMed: 18156677]

24. Langer G, Cohen SX, Lamzin VS, Perrakis A. Automated macromolecular model building for X-ray crystallography using ARP/wARP version 7. Nat Protoc. 2008; 3:1171–1179. [PubMed: 18600222]

25. Emsley P, Cowtan K. Coot: model-building tools for molecular graphics. Acta Crystallographica, Section D: Biological Crystallography. 2004; D60:2126–2132.

26. Murshudov GN, Vagin AA, Dodson EJ. Refinement of macromolecular structures by the maximum-likelihood method. Acta Crystallographica, Section D: Biological Crystallography. 1997; D53:240–255.

27. Pettersen EF, Goddard TD, Huang CC, Couch GS, Greenblatt DM, Meng EC, Ferrin TE. UCSF Chimera-A visualization system for exploratory research and analysis. J Comput Chem. 2004; 25:1605–1612. [PubMed: 15264254]

28. Schuttelkopf AW, van ADMF. PRODRG: a tool for high-throughput crystallography of protein-ligand complexes. Acta Crystallogr D Biol Crystallogr. 2004; 60:1355–1363. [PubMed: 15272157]

29. Pakhomova S, Rife CL, Armstrong RN, Newcomer ME. Structure of fosfomycin resistance protein FosA from transposon Tn2921. Protein Sci. 2004; 13:1260–1265. [PubMed: 15075406]

30. Armstrong RN. Mechanistic diversity in a metalloenzyme superfamily. Biochemistry. 2000; 39:13625–13632. [PubMed: 11076500]

31. Bernat BA, Laughlin LT, Armstrong RN. Regiochemical and Stereochemical Course of the Reaction Catalyzed by the Fosfomycin Resistance Protein, FosA. J Org Chem. 1998; 63:3778–3780.

32. Roberts AA, Sharma SV, Strankman AW, Duran SR, Rawat M, Hamilton CJ. Mechanistic studies of FosB: a divalent-metal-dependent bacillithiol-S-transferase that mediates fosfomycin resistance in Staphylococcus aureus. Biochem J. 2013; 451:69–79. [PubMed: 23256780]

33. Rigsby RE, Brown DW, Dawson E, Lybrand TP, Armstrong RN. A model for glutathione binding and activation in the fosfomycin resistance protein, FosA. Arch Biochem Biophys. 2007; 464:277–283. [PubMed: 17537395]

34. Pearson RG. Hard and soft acids and bases (HSAB). I. Fundamental principles. J Chem Educ. 1968; 45:581–587.

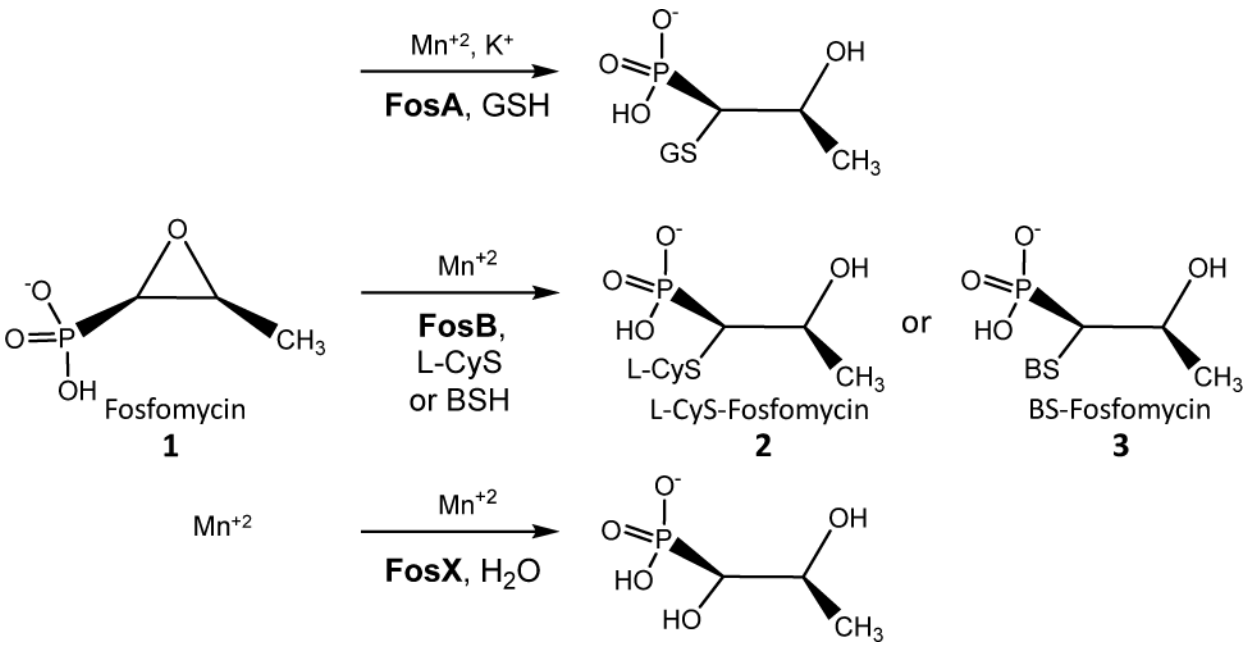

Figure 1.

Reactions catalyzed by the fosfomycin resistance proteins FosA, FosB and FosX. FosA is a Mn^{+2} and K^{+}-dependent GSH transferase. FosB is a Mn^{2+} dependent L-cysteine or bacillithiol (BSH) transferase. FosX is a Mn^{+2} dependent hydrolase. All three enzymes catalyze nucleophilic addition to the C1 of fosfomycin subsequently opening the epoxide ring destroying the efficacy of the drug.

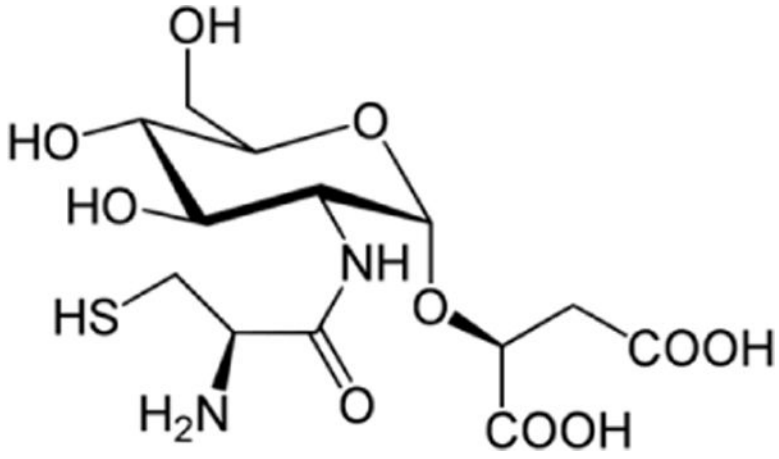

Figure 2.
Structure of bacillithiol

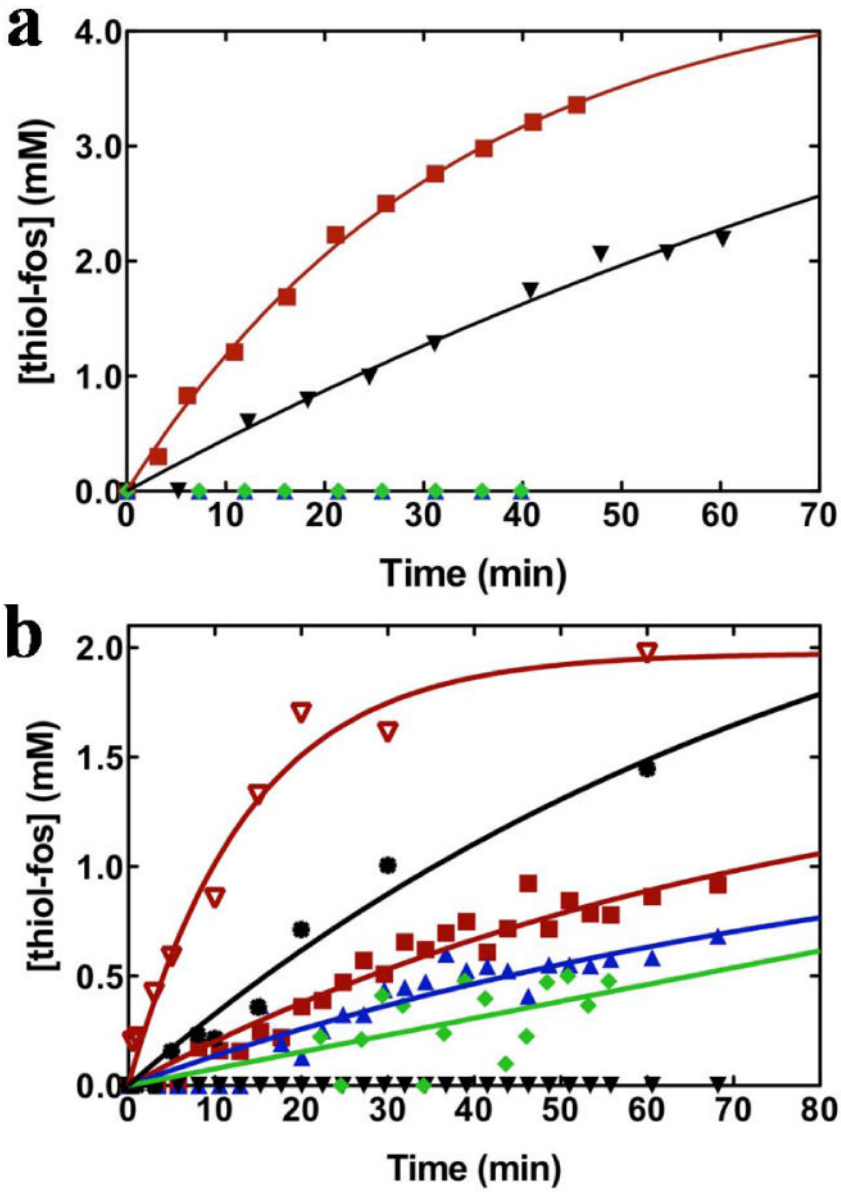

Figure 3.

(a) Time course kinetics for FosB^{Bc} catalyzed-addition of BSH or L-cys to fosfomycin in the presence of Mg^{2+} or Zn^{2+}. Reactions were carried out at 25° C in 20 mM HEPES, pH 7.0 with 8 mM fosfomycin and 0.5 μM enzyme in the presence of (■) 4 mM BSH and 10 mM Mg^{2+}, (▼) 4 mM L-cys and 10 mM Mg^{2+}, (▲) 4 mM BSH and 100 μM Zn^{2+}, or (◆) 4 mM L-Cys and 100 μM Zn^{2+}. **(b)** Time course of FosB^{Bc} catalyzed-addition of BSH or L-cys to fosfomycin in the presence of Mg^{2+}, Ni^{2+}, or Mn^{2+}. Reactions were carried out at 25° C in 20 mM HEPES, pH 7.0 with 4 mM fosfomycin and 0.25 μM enzyme in the presence of (▽) 2 mM BSH and 10 μM Mn^{2+}, (■) 2 mM BSH and 10 μM Ni^{2+}, (▲) 2 mM BSH and 1 mM Mg^{2+}, (●) 2 mM L-cys and 10 μM Mn^{2+}, (▼) 2 mM L-Cys and 10 μM Ni^{2+} or (◆) 2 mM L-Cys and 1 mM Mg^{2+}.

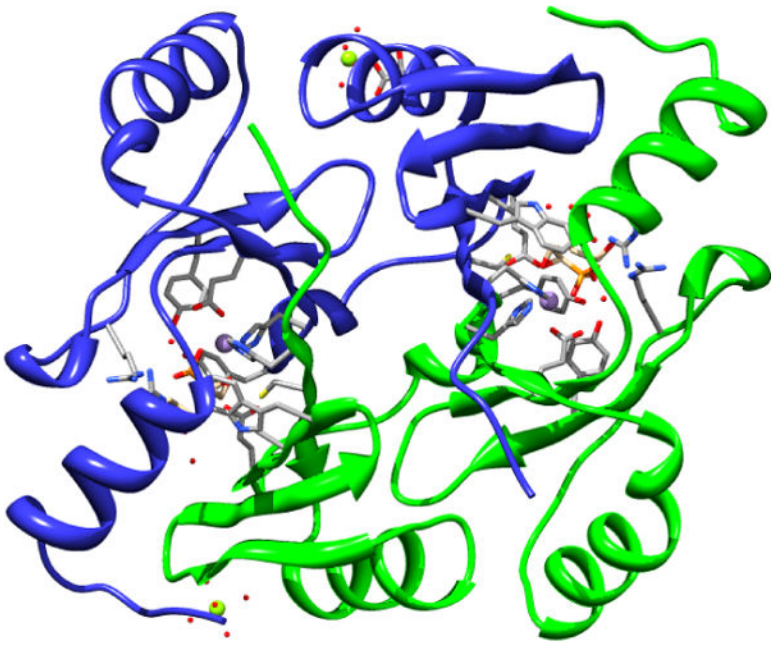

Figure 4.

Overall x-ray crystal structure of the FosB protein from *Bacillus cereus* in complex with Mn^{2+} and fosfomycin at 1.32 Å-resolution (PDB 4JH6). Final refinement had an R_{work} = 13.79% and R_{free} = 17.05%.

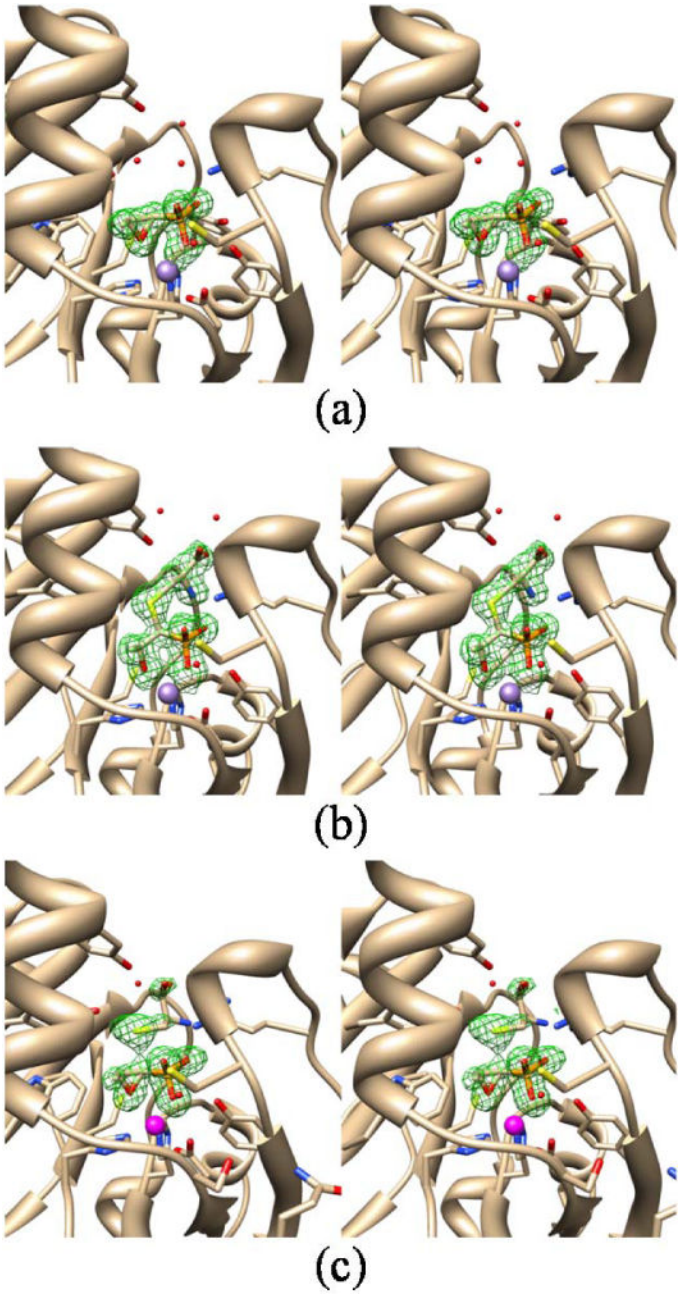

Figure 5.

Stereo views of (a) FosB^{Bc}•Mn^{2+}•**1** (PDB 4JH6), (b) FosB^{Bc}•Mn^{2+}•**2** (PDB 4JH7), and (c) FosB^{Bc}•Zn^{2+}•**1**•L-cys (PDB 4JH8). Difference densities are the $2F_o$-F_c maps calculated before addition of the ligands to the coordinate files and are contoured at 3σ. The electron density in (a) shows the position of **1** coordinated to Mn^{2+}. The electron density in (b) clearly shows **2** coordinated to Mn^{2+}, and the density for C1 of **1** is sp^3 hybridized following nucleophilic attack by the L-cys thiol. The electron density in (c) shows **1** coordinated to Zn^{2+} with the density for the C1 carbon of **1** more substrate-like in geometry than that of (b), indicating no product formation. The strong electron density above C1 likely belongs to

sulfur. The ambiguity in the rest of the density for the L-cys is probably due to a combination of occupancy and multiple conformations in the crystal.

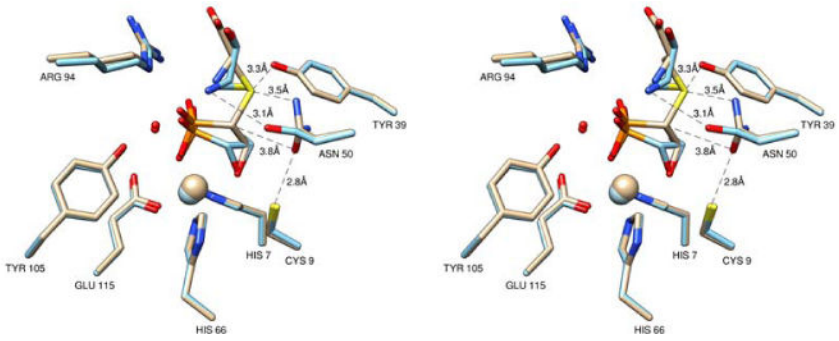

Figure 6.

Stereo view for superposition of the FosB^{Bc}•Mn^{2+}•**2** structure (PDB 4JH7) and the FosB^{Bc}•Zn^{2+}•**1**•L-cysteine ternary structure (PDB 4JH8). While the positions of all other amino acids stay the same, Asn50 in the ternary complex is rotated approximately 90 degrees relative to the product complex. Rotation of Asn50 about the C_β-C_γ bond is the only significant difference observed in the reported structures of FosB^{Bc}. The conserved residues, Tyr39 and Asn50, likely work in a concerted manner to ionize and stabilize the approaching thiolate during nucleophilic attack of the antibiotic.

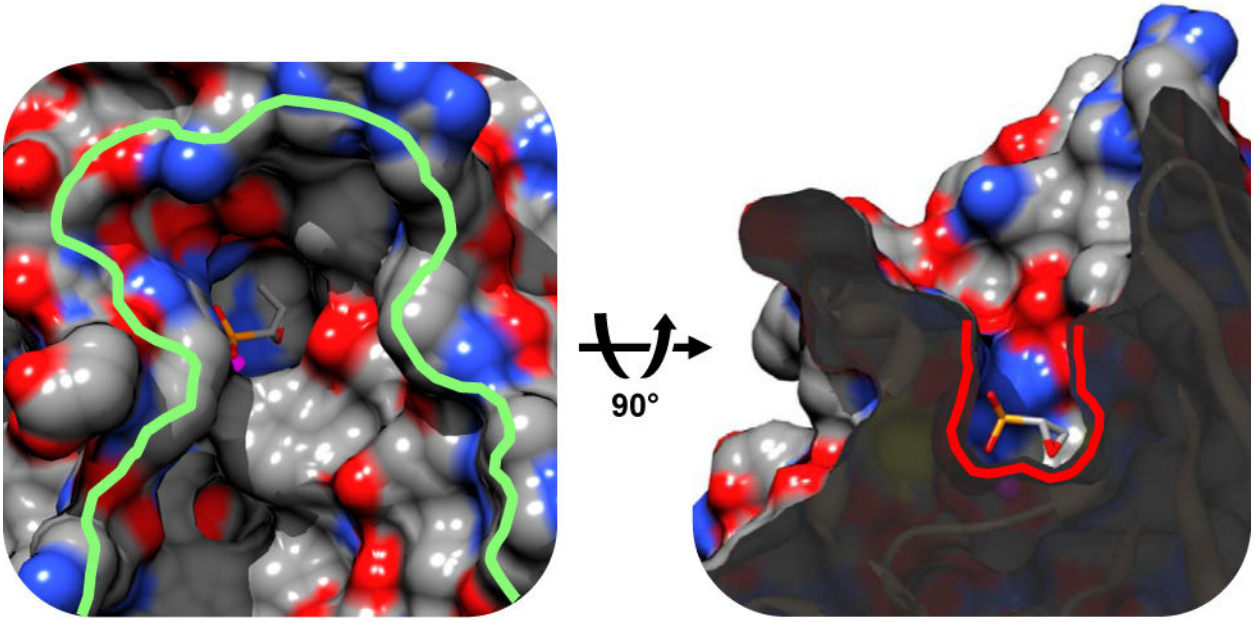

Figure 7.

The **left** panel shows the top-view of a channel from the surface of the protein into the active site. The green line contours a depression in the surface of the protein large enough to accommodate BSH. The **right** panel illustrates the narrowing of the channel near fosfomycin (shown in stick representation). The narrow section (outlined in red) is large enough to accommodate either L-Cys or the cysteinyl-moiety of BSH. Note that the backside of the oxirane carbon to be attacked is positioned in the middle of the solvent channel. Figure made with PDB 4JH3.

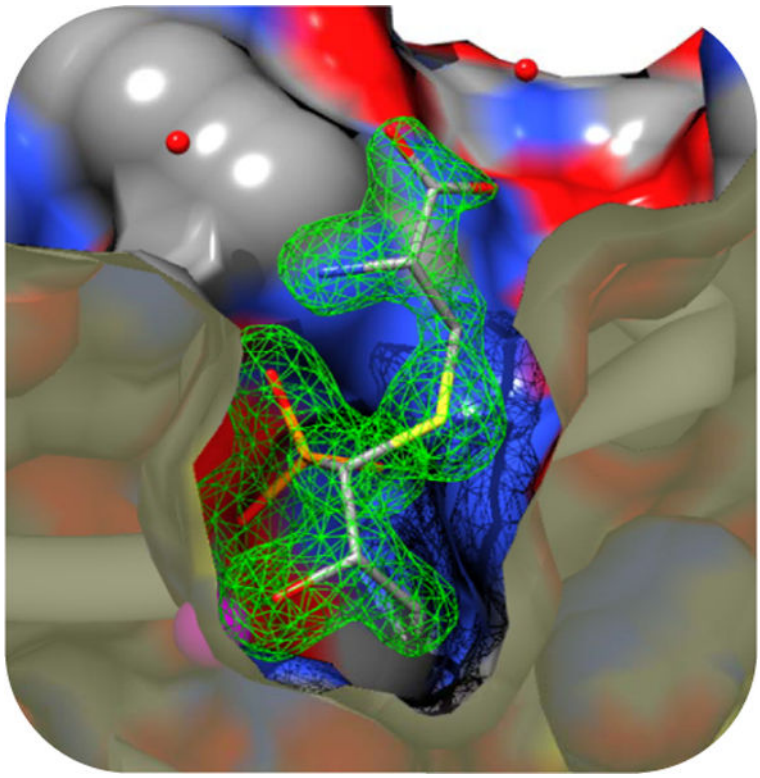

Figure 8.

The active site of FosB^{Bc} in complex with Mn^{2+} and **2**, (1R,2S)-1-(S-L-cysteinyl)-2-hydroxypropylphosphonate, at 1.55 Å resolution (PDB 4JH7). Final refinement had an R_{work} =13.33% and R_{free} = 18.64%. The difference electron density shown for **2** is the $2F_o$-F_c map calculated before addition of **2** to the coordinate file. It is contoured at 3σ and emphasizes the quality of the data. The C1 of fosfomycin is clearly sp^3 hybridized and strong electron density is observed for the sulfur.

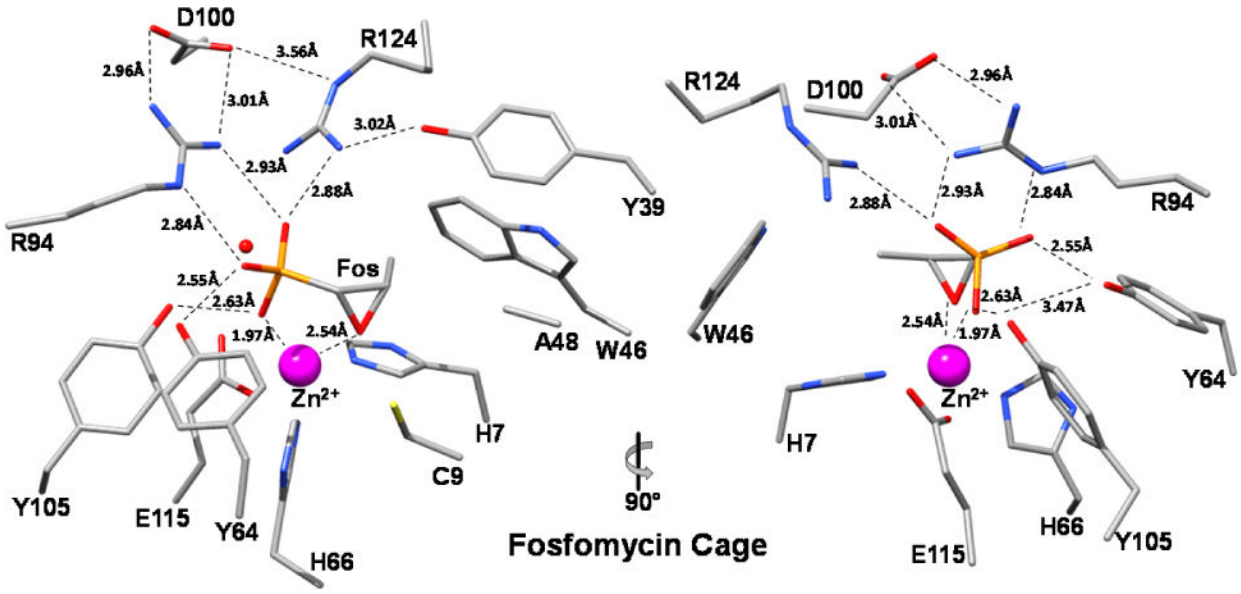

Figure 9.

The fosfomycin molecule is surrounded by a cage of amino acids. The cage has both a polar and non-polar end to accommodate the antibiotic. The polar phosphonate group is coordinated to the metal through one of the phosphonate oxygens and hydrogen bonded to Arg94, Arg124, Tyr64, and Tyr105 through the other two. On the opposite end, the oxirane oxygen is coordinated to the metal and the hydrophobic methyl group of fosfomycin is held adjacent to Trp46. The amino acids that construct the fosmomycin cage are conserved throughout all of the FosB enzymes (see Figure S10, Green). Figure made with PDB 4JH3.

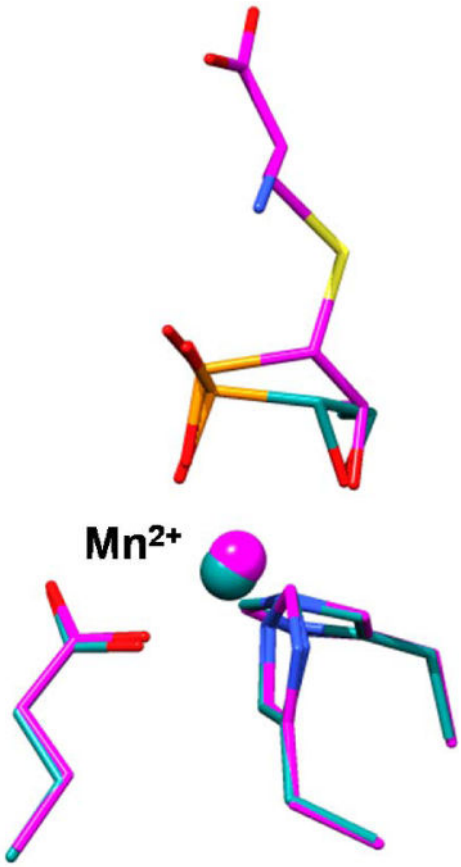

Figure 10.

Superposition of the FosB^{Bc}•Mn^{2+}•**1** (PDB 4JH6) and FosB^{Bc}•Mn^{2+}•**2** (PDB 4JH7) structures. When the L-cys thiol adds to C1 of fosfomycin and the epoxide ring opens, the Mn^{2+} metal displaces from the three coordinating amino acids such that the overall coordination geometry of Mn^{2+} changes. Specifically, the equatorial distances expand, and the metal-oxygen$_{(oxirane)}$ bond shortens, effectively creating a more symmetric trigonal bipyramidal geometry around Mn^{2+} and relieving strain on both the atomic orbitals of the metal and the epoxide ring of the antibiotic (see Table 2).

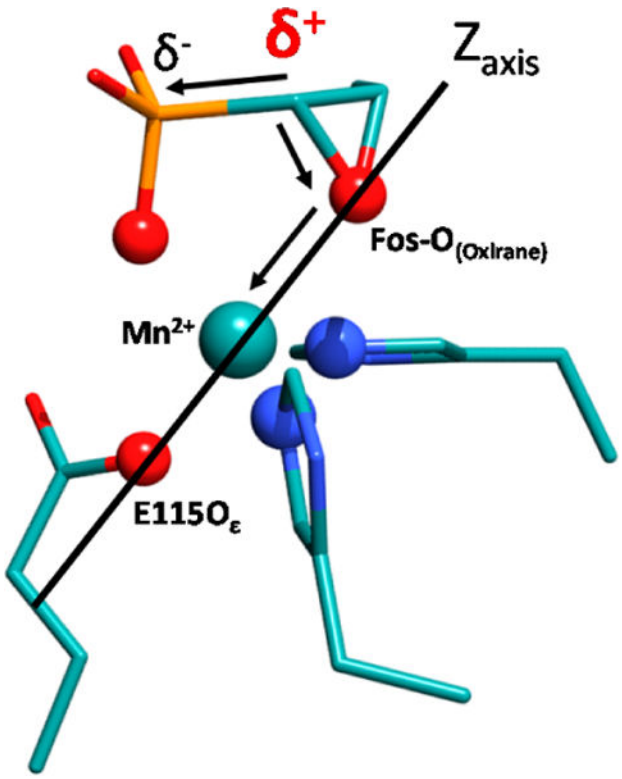

Figure 11.

The activation of fosfomycin occurs through σ donation of the epoxide lone pair into the d_z^2 orbital of Mn^{2+}, significantly increasing the polarity of the C1-O(Oxirane) bond and resulting in greater partial positive charge (δ^+) on C1. In addition, the electron withdrawing nature of the phosphonate group will further enhance δ^+ on C1 through polarization of the C1-P bond. Arrows denote electron charge redistribution away from C1 to both the phosphonate and the epoxide oxygen. This primes the antibiotic for nucleophilic attack by the thiol substrate. Figure made with PDB 4JH6.

Table 1

Data Collection and Refinement Statistics for FosB^{Bc}

	FosB•Zn•Sulf SAD	FosB•Zn•Sulf MR	FosB•Zn•Fos SAD	FosB•Ni•Fos SAD	FosB•Co•Fos SAD	FosB•Mn•Fos MR	FosB•Mn•Cys-Fos MR	FosB•Zn•Cys-Fos MR	FosBMn•BSH•Fos MR
PDB code	4JH1	4JH2	4JH3	4JH4	4JH5	4JH6	4JH7	4JH8	4JH9
Space group	$P\,2_12_12_1$	$P\,2_12_12_1$	$P\,2_12_12_1$	$P\,2_12_12_1$	$P\,2_12_12_1$	$P\,2_12_12_1$	$P\,2_12_12_1$	$P\,2_12_12_1$	$P\,2_12_12_1$
Unit-cell parameters									
a (Å)	64.45	64.34	64.34	64.41	64.33	64.49	64.29	64.31	56.48
b (Å)	68.20	68.09	68.27	68.54	68.23	68.69	68.31	68.54	64.48
c (Å)	69.60	69.77	69.90	70.44	69.88	70.09	70.18	69.85	83.91
Data collection									
Temperature (K)	100	100	100	100	100	100	100	100	100
Wavelength (Å)	1.2823	1.0781	1.2823	1.4847	1.6046	1.1272	1.0781	1.0781	1.1272
Resolution (Å)[a]	48.71−1.55 (1.61−1.55)	48.73−1.27 (1.29−1.27)	48.84−1.50 (1.55−1.50)	49.12−1.89 (1.93−1.89)	48.82−1.77 (1.80−1.77)	49.06−1.32 (1.34−1.32)	48.95−1.55 (1.58−1.55)	48.92−1.41 (1.43−1.41)	51.13−1.77 (1.83−1.77)
Unique reflections	44556	81296	49820	25035	30425	72030	44593	59747	30311
Completeness (%)[a]	98.3 (85.2)	99.8 (99.2)	98.8 (94.2)	98.4 (97.0)	98.8 (95.6)	97.8 (99.9)	97.9 (95.6)	99.1 (97.6)	99.2 (92.7)
R_{merge}(%)[b]	9.3 (52.9)	7.6 (36.1)	9.5 (60.3)	12.6 (79.2)	9.5 (39.8)	5.1 (54.8)	6.6 (45.3)	4.8 (56.2)	8.4 (60.1)
I/σ	27.5 (2.8)	46.0 (5.8)	23 (3.3)	36.6 (5.4)	64.2 (9.0)	32.19 (2.0)	30.1 (3.6)	43.5 (3.0)	12.0 (2.1)
Redundancy	8.5 (4.7)	7.1 (7.0)	9.3 (7.1)	14.2 (14.1)	13.3 (13.0)	4.0 (3.7)	7.4 (7.3)	7.3 (7.1)	4.7 (4.4)
Refinement									
R_{work}/R_{free}(%)[c]	13.33/18.78	12.41/15.16	12.36/16.83	17.22/21.62	16.94/20.93	13.79/17.05	13.33/18.64	13.72/17.41	18.30/23.55
Figure of merit (%)	90.25	93.69	91.79	87.48	87.94	91.01	91.13	92.02	82.16
Average B factor (Å^2)									
All atoms	18.17	14.80	17.67	19.28	17.33	20.38	15.67	19.74	26.37
Protein	17.01	13.34	16.25	19.03	16.90	19.62	14.55	18.66	26.15
Water	28.59	24.20	28.25	23.53	22.77	26.82	23.11	26.83	28.67
No. of atoms									
Protein	2640	2938	2707	2484	2546	2702	2682	2751	2524
Water	258	379	315	142	185	250	259	253	135
Rmsd from ideal									
Bond length (Å)	0.021	0.023	0.021	0.020	0.023	0.023	0.021	0.023	0.019

	FosB•Zn•Sulf SAD	FosB•Zn•Sulf MR	FosB•Zn•Fos SAD	FosB•Ni•Fos SAD	FosB•Co•Fos SAD	FosB•Mn•Fos MR	FosB•Mn•Cys-Fos MR	FosB•Zn•Cys-Fos MR	FosBMn•BSH•Fos MR
Bond angle (deg)	1.96	2.28	1.95	2.02	2.20	2.20	2.07	2.30	1.97
Ramachandran plot (%)[d]									
Most favored	234	234	234	235	234	234	232	232	230
Allowed	16	16	16	15	16	16	18	18	20
Disallowed	2	2	2	2	2	2	2	2	2

[a] Values in parentheses are for the highest resolution shell.

[b] Rmerge =Σ(|I−Ī|)/ΣI×100.

[c] Rwork = Σ|Fo−Fc|/ΣFo ×100, where Fo is the observed structure factor amplitude and Fc is the calculated structure factor amplitude.

[d] Values are given as number of residues.

Table 2

Metal-Ligand Distances for FosB^{Bc} •Mn^{2+}•**1** and FosB^{Bc} •Mn^{2+}•**2**. (Å)

Structure	Mn^{2+}-H7$_{N\varepsilon}$	Mn^{2+}-H66$_{N\varepsilon}$	Mn^{2+}-E115$_{O\varepsilon}$	Mn^{2+}-O$_{(Phosphonate)}$	Mn^{2+}-O$_{(Oxirane)}$
FosB^{Bc} •Mn^{2+}•**1**	2.08	2.03	2.04	1.91	2.51
FosB^{Bc} •Mn^{2+}•**2**	2.16	2.17	2.07	2.01	2.38